Surface & Coatings Technology 265 (2015) 16–23

Contents lists available at ScienceDirect

Surface & Coatings Technology

journal homepage: www.elsevier.com/locate/surfcoat

# Influence of carbon concentration on the electrochemical behavior of CrCN coatings in simulated body fluid

Qianzhi Wang [a,b,c,e], Fei Zhou [a,b,e,*], Zhifeng Zhou [d], Lawrence Kwok-Yan Li [d], Jiwang Yan [c]

[a] State Key Laboratory of Mechanics and Control of Mechanical Structures, Nanjing University of Aeronautics and Astronautics, Nanjing 210016, China
[b] College of Mechanical and Electrical Engineering, Nanjing University of Aeronautics and Astronautics, Nanjing 210016, China
[c] Department of Mechanical Engineering, Faculty of Science and Technology, Keio University, Yokohama 2238522, Japan
[d] Advanced Coatings Applied Research Laboratory, Department of Mechanical and Biomedical Engineering, City University of Hong Kong, 83 Tat Chee Avenue, Kowloon, Hong Kong, China
[e] Jiangsu Key Laboratory of Precision and Micro-Manufacturing Technology, Nanjing 210016, China

ARTICLE INFO

*Article history:*
Received 7 October 2014
Accepted in revised form 29 January 2015
Available online 7 February 2015

*Keywords:*
CrCN coatings
Electrochemical properties
Simulated body fluid
EIS
Polarization

ABSTRACT

CrCN coatings with various carbon contents were deposited on 316 L stainless steel disks by unbalanced magnetron sputtering via adjusting carbon target current, and their relevant microstructure was characterized by Raman spectrum and X-ray photoelectron spectroscopy, respectively. The influence of carbon content on the electrochemical properties of CrCN coatings in simulated body fluid (SBF) was investigated using open circuit potential (OCP), electrochemical impedance spectroscopy (EIS) and potentiodynamic polarization tests. It turned out that the CrCN-coated 316 L disks performed better electrochemical properties than uncoated 316 L disk. All CrCN coatings contained a-$CN_x$, but the bonding structure converted from N–C bonds to N═C bonds as carbon content increased. As a result, the CrCN coatings (52.6–75.0 at.% C) with N═C bonds were prone to be easily degraded by breakage of π bond. In contrast, the CrCN coatings (15.4 at.% C) with N–C bond alone exhibited relatively higher charge transfer resistance ($R_{ct}$), and was able to prolong the longevity of prosthesis.


## 1. Introduction

On account of cheap price, free of magnetism and excellent ductility, prosthesis made of 316 L stainless steel has accounted for a major portion in surgical prosthesis market [1,2]. Nevertheless, 316 L stainless steel still confronted unsatisfactory service life resulting from local corrosion, fretting fatigue and formation of fibrous tissue in physiological environment [3–7], which led to about 10% of hip arthroplasties being substituted after 10–15 years [8–10]. In order to prolong the longevity of femoral head prosthesis made of 316 L stainless steel, some advanced compound coatings such as metal or non-metal incorporated a-C and TiCN coatings [11–16] have been applied to modify its surface characteristics. Recently, CrCN coatings have been paid more attention due to lower internal stress, higher hardness and superior tribological property [17,18]. Meanwhile, their electrochemical behavior has been investigated in different environments. Yi et al. [19] pointed out that CrCN coatings exhibited better protection effect than CrN coatings when immersed in 0.5 M $H_2SO_4$ and 5 ppm HF solution. Similarly, Merl et al. [20] manifested that carbon incorporation could enhance the inhibition ability of CrCN coatings on SS304 in 0.5 M NaCl solution, whereas the opposite result on K340 in 0.5% NaCl solution was reported by Kaciulis et al. [21]. It is worth noting that the carbon concentration of CrCN coatings in Ref. [20] has not been reported, while that of CrCN coatings in Ref. [21] varied in the range of 55.4 at.% to 65 at.%. Thus, the totally contradictory results in Refs. [20,21] might be caused by the different carbon concentrations. In other words, the electrochemical properties of CrCN coatings were strongly dependent on carbon concentration. However, the influence of carbon concentration on the electrochemical properties of CrCN coatings in SBF has not yet been investigated systematically.

In here, the CrCN coatings with varied carbon concentrations (15.4–75.0 at.%) were deposited on 316 L steel disks using unbalanced magnetron sputtering via adjusting the carbon target current. The electrochemical characteristics of CrCN coatings in SBF were investigated using open circuit potential (OCP), electrochemical impedance spectroscopy (EIS) and potentiodynamic polarization tests, and then the influence of carbon concentration on the electrochemical characteristics of CrCN coatings in SBF was outlined.

## 2. Experiment details

### 2.1. Fabrication of CrCN coatings

316 L disks with composition in Table 1 were selected as substrates (Ø30 × 4 mm), and polished to a roughness ($R_a$) of 30 nm by a

* Corresponding author at: State Key Laboratory of Mechanics and Control of Mechanical Structures, Nanjing University of Aeronautics and Astronautics, Nanjing 210016, China. Tel./fax: +86 25 84893083.
*E-mail address:* fzhou@nuaa.edu.cn (F. Zhou).

http://dx.doi.org/10.1016/j.surfcoat.2015.01.068
0257-8972/

**Table 1**
Specific chemical composition of 316 L stainless steel.

| Composition | C | Si | Mn | P | S | Ni | Cr | Mo | Fe |
|---|---|---|---|---|---|---|---|---|---|
| Mass fraction (wt.%) | 0.02 | 0.65 | 1.70 | 0.03 | 0.01 | 12.0 | 17.5 | 2.5 | Balanced |

**Table 2**
Deposition parameters of CrN and CrCN coatings.

| Parameter | Figure | Thickness |
|---|---|---|
| Chamber pressure | 0.23 Pa | – |
| Temperature | Room temperature | – |
| Bias voltage | −60 V | – |
| Rotating speed of holder | 10 rpm | – |
| Current of chromium target | 8 A | – |
| Current of graphite target | 0 A CrN | 1.00 μm |
| | 1 A CrCN(1) | 1.04 μm |
| | 2 A CrCN(2) | 1.74 μm |
| | 3 A CrCN(3) | 2.19 μm |

metallographic polishing machine (UNIPOL-820). After being ultrasonically cleaned in ethanol and deionized water, they were fixed on the holder inside a chamber. Before deposition, $Ar^+$ plasma at a bias voltage of −450 V was applied to intensively clean and activate 316 L disks for 30 min. Under an atmosphere of Ar and $N_2$ gases, CrCN coatings were fabricated by sputtering chromium and graphite targets simultaneously (UDP-650, Teer Coatings Limited, UK). In this case, a pure Cr adhesive layer (about 0.2 μm) was deposited beforehand to enhance adhesive strength, and the detailed deposition parameters are listed in Table 2. In next section, the CrCN coatings deposited at the graphite target currents of 1A, 2A and 3A would be denoted as CrCN(1), CrCN(2) and CrCN(3) coatings, while pure CrN coating was also deposited for comparison.

### 2.2. Microstructure characterization of CrCN coatings

The morphology and thickness of CrCN coatings were observed and measured using a field emission scanning electron microscope (FE-SEM) (Philips FEG-XL30), while bonding structure and composition were characterized via Raman spectroscopy (InVia 2000, Renishaw) and X-ray photoelectron spectroscopy (XPS, VG ESCALAB 220-iXL Al Kα), respectively. The excitation wavelength of Raman spectroscopy was 514 nm with exposure time of 10 s, and the power of the excitation was 2.60 mW with a spot diameter of 1 μm. As regards XPS, the spectra were deconvoluted with XPS PEAK 4.1 software with the reference energy of 284.8 eV for $C_{1s}$ peak. Then, the corresponding $N_{1s}$ spectrum was fitted under a Shirley background type, and the ratio of Lorentzian to Gaussian was 20%. Besides, the electrical resistivities of CrCN-coated and uncoated 316 L disks were measured by a four point probe technique (KDY-1, KunDe Technology Co., Ltd.).

### 2.3. Electrochemical tests of CrCN coatings

A standard three-electrode electrochemical cell was used, which consisted of a saturated calomel reference electrode (SCE), a platinum wire counter electrode and working electrodes of specimens. At first, open circuit potential (OCP) was recorded immediately since the immersion of specimen in SBF. When OCP measurement had been done for 1 h, electrochemical impedance spectroscopy (EIS) was conducted at OCP with an AC excitation of 10 mV from 1 mHz to 100 kHz. The duration of each EIS measurement lasted for about 2.5 h, and the EIS measurement was repeated for three times by using a new sample in fresh solution to ensure the reliability of the data.

**Table 4**
Element concentrations detected by XPS and electrical resistivities measured by four point probe technique for different samples.

| Samples | Cr (at.%) | C (at.%) | N (at.%) | Electrical resistivity ($\Omega\cdot mm^2/m$) |
|---|---|---|---|---|
| 316 L | – | – | – | 0.71 |
| CrN | 60.1 | 0.00 | 39.9 | 0.66 |
| CrCN(1) | 64.2 | 15.4 | 20.4 | 0.75 |
| CrCN(2) | 23.1 | 52.6 | 24.3 | 0.94 |
| CrCN(3) | 9.5 | 75.0 | 15.5 | 0.82 |

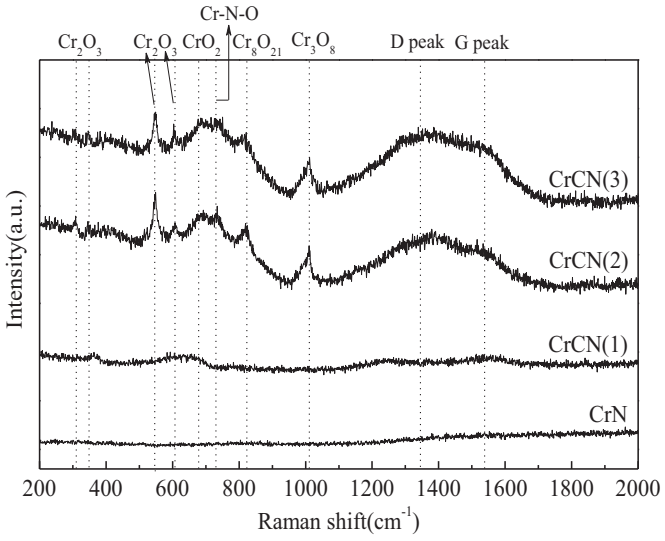


**Fig. 1.** Raman spectra of CrCN coatings deposited at different graphite target currents.

$$C = -\frac{i}{\omega Z''} = -\frac{i}{2\pi f Z''}. \quad (1)$$

Then, interfacial capacitance $C$ was obtained using Eq. (1), where $Z''$ is the imaginary part of impedance, and $f$ is the AC frequency in Hertz [22]. Subsequently, potentiodynamic polarization test was carried out by polarizing specimens in anodic direction from −0.8 V to 0.8 V with a sweep rate at 20 mV/min, and each polarization test lasted for about 1.4 h. All the above-mentioned measurements were carried out at room temperature in simulated body fluid (SBF) with pH 7.4, of which the detailed formula is listed in Table 3 [23]. After measurement, EIS data were fitted according to equivalent circuit via ZsimpWin software. Besides, corrosion potential ($E_{corr}$) and corrosion current density ($j_{corr}$) were deduced from the Tafel plot via extrapolation method.

$$R_p = \frac{\beta_a \beta_c}{2.303 j_{corr}(\beta_a + \beta_c)} \quad (2)$$

Then polarization resistance ($R_p$) was obtained using Stern–Geary Eq. (2) [24,25], where the $\beta_a$ and $\beta_c$ are the Tafel anodic and cathodic slopes.

**Table 3**
Formula of simulated body fluid.

| Compound | NaCl | $NaHCO_3$ | KCl | $K_2HPO_4\cdot 3H_2O$ | $MgCl_2\cdot 6H_2O$ | $CaCl_2$ | $Na_2SO_4$ | $(CH_2OH)_3CNH_2$ |
|---|---|---|---|---|---|---|---|---|
| Concentration (g/L) | 7.996 | 0.35 | 0.22 | 0.228 | 0.305 | 0.278 | 0.071 | 6.057 |

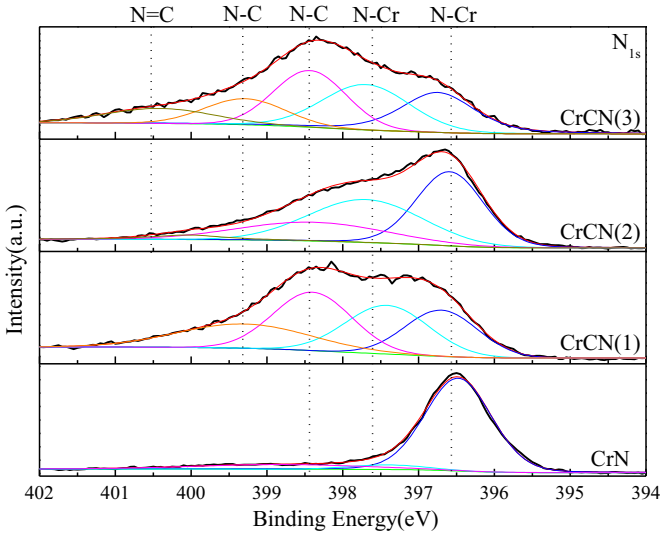


**Fig. 2.** $N_{1s}$ core XPS spectra of CrCN coatings deposited at different graphite target currents.

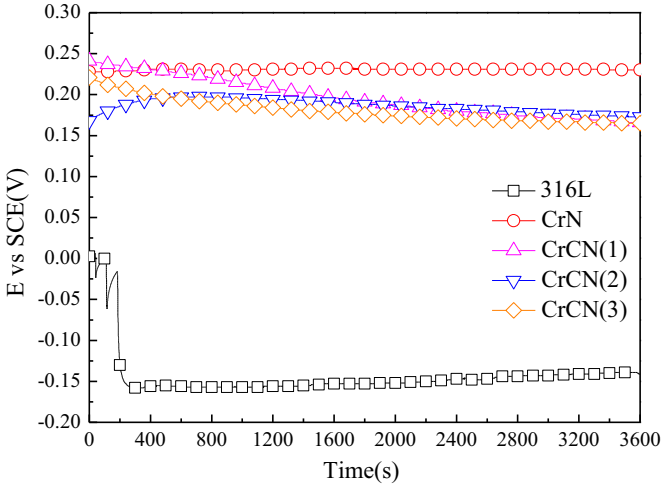


**Fig. 4.** OCPs of the coated and uncoated 316 L disks.

**Table 5**
Volume fractions of different bonds from $N_{1s}$ XPS results of CrCN coatings.

| Coatings | N–Cr (%) (CrN) | N–C (%) (a-$CN_x$) | N=C (%) (a-$CN_x$) |
|---|---|---|---|
| CrCN(1) | 48.7 | 51.3 | 0.00 |
| CrCN(2) | 75.7 | 20.9 | 3.40 |
| CrCN(3) | 49.2 | 40.2 | 10.6 |

## 3. Results and discussion

### 3.1. Microstructure characterization of CrCN coatings

The element concentration of CrCN coatings is listed in Table 4 according to XPS analyses. It is clear that the concentration of C atom raised drastically from 15.4 at.% to 75.0 at.%, while those of Cr and N atoms decreased from 64.2 at.% to 9.5 at.% and from 20.4 at.% to 15.5 at.% when the graphite target current increased from 1 A to 3 A. Taking the thickness of CrCN coatings into account (Table 2), it is implied that when the current of graphite target exceeded 1 A, the deposition rate of carbon increased sharply. Thus, the concentration of C atom drastically rose to 52.6 at.% and 75.0 at.% while the thicknesses of CrCN(2) and CrCN(3) coatings enhanced to 1.74 μm and 2.19 μm.

As seen in Fig. 1, only the Raman spectra of CrCN(2) and CrCN(3) coatings exhibited the obvious signs of D (disordered carbon) and G (graphitic carbon) peaks which were centered around 1350 and 1580 $cm^{-1}$. In addition, seven peaks at 305, 346, 547, 610, 684, 820 and 1009 $cm^{-1}$ originated from various chromium oxides [26–30], and one peak at 727 $cm^{-1}$ stemmed from Cr–N–O simultaneously

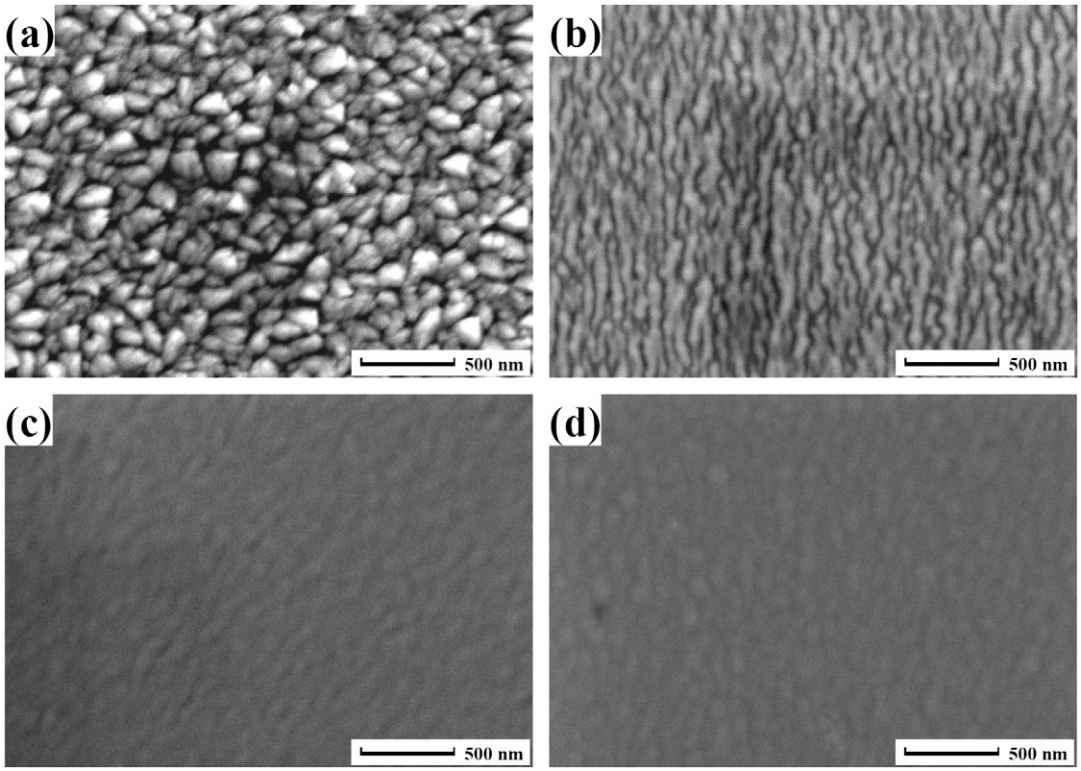


**Fig. 3.** Topographies of (a) CrN, (b) CrCN(1), (c) CrCN(2), and (d) CrCN(3) coatings.

**Table 6**
Characteristics of the equivalent circuits derived from the EIS spectra in SBF.

| Samples | $R_s$ ($\Omega$ cm$^2$) | $(CPE\text{-}Y_o)_{po}$ (Fcm$^{-2}$) | $(CPE\text{-}n)_{po}$ | $R_{po}$ ($\Omega$ cm$^2$) | $(CPE\text{-}Y_o)_{dl}$ (Fcm$^{-2}$) | $(CPE\text{-}n)_{dl}$ | $R_{ct}$ ($\Omega$ cm$^2$) |
|---|---|---|---|---|---|---|---|
| 316 L | 11.1 | – | – | – | $2.36 \times 10^{-5}$ | 0.920 | $6.69 \times 10^5$ |
| CrN | 16.23 | $1.47 \times 10^{-5}$ | 0.975 | $1.85 \times 10^2$ | $4.35 \times 10^{-5}$ | 0.701 | $3.22 \times 10^6$ |
| CrCN(1) | 3.40 | $8.39 \times 10^{-6}$ | 0.711 | $9.51 \times 10^1$ | $1.38 \times 10^{-6}$ | 0.996 | $5.33 \times 10^7$ |
| CrCN(2) | 1.20 | $8.56 \times 10^{-8}$ | 0.995 | $3.25 \times 10^1$ | $8.60 \times 10^{-6}$ | 0.925 | $3.35 \times 10^7$ |
| CrCN(3) | 7.90 | $2.68 \times 10^{-7}$ | 0.992 | $1.26 \times 10^1$ | $2.36 \times 10^{-5}$ | 0.995 | $8.06 \times 10^6$ |

[31]. It is indicated that the carbon concentrations in CrCN(2) and CrCN(3) coatings were rich enough to form amorphous carbon, but the chromium oxides might be resulted from residual oxygen in the chamber or oxygen contamination in air. In order to further understand the bonding structure of CrCN coatings, the $N_{1s}$ XPS spectra of CrCN coatings are illustrated in Fig. 2. It is worth noting that, after incorporating C element into CrN coating, N atom not only bonded with Cr atom but also bonded with C atom to form N–C bonds at 398.4 eV and 399.3 eV and N═C bond at 400.4 eV [32]. According to individual area, the volume fraction of each bond was calculated and is listed in Table 5. It is conspicuous that CrCN(1) coating only exhibited N–C bond with the volume fraction of 51.3%. However, the volume fractions of N–C and N═C bonds in the CrCN(2) coating were 20.9% and 3.4%, while those in the CrCN(3) coatings increased to 40.2% and 10.6%. It is indicated that when the carbon concentration was 15.4 at.%, CrCN(1) coating mainly composed of CrN and a-$CN_x$ with N–C bond alone. But as carbon concentrations increased to 52.6 at.% and 75.0 at.%, the CrCN(2) and CrCN(3) coatings consisted of CrN, a-C and a-$CN_x$ with N–C and N═C bonds, especially, CrCN(3) coating contained more N═C bonds [18].

The topographies of CrCN coatings are shown in Fig. 3, and CrN coating exhibited rice grain-like morphology with many obvious gaps. When the current of graphite target increased to 1 A, CrCN(1) coating presented short line-like and dense topography. Subsequently, CrCN(2) and CrCN(3) coatings displayed more compact surface profiles which resulted from the formation of amorphous carbon. Under the interactive effects of bonding structure and topography, the electrical resistivity in Table 4 increased from 0.66 $\Omega \cdot mm^2/m$ for CrN coating to 0.94 $\Omega \cdot mm^2/m$ for CrCN(2) coating due to the formation of a-$CN_x$. However, the more a-C in CrCN(3) coating made the electrical resistivity drop to 0.82 $\Omega \cdot mm^2/m$ [18].

### 3.2. Influence of carbon concentration on the OCP of CrCN coatings

As seen in Fig. 4, the OCP of uncoated 316 L disk exhibited a sharp drop during the first 200 s, which indicated the occurrence of pitting corrosion [33], but all CrCN-coated 316 L disks displayed steady OCPs during whole immersion process, which demonstrated the inhibition effects of CrCN coatings on pitting.

$$2CrN + 3H_2O = Cr_2O_3 + 2NH_3 \qquad \Delta G_f^{298} = -250 \cdot 10\ \text{kJ} \cdot \text{mol}^{-1} \tag{3}$$

In addition, the OCPs of CrCN-coated 316 L disks were all higher than those of uncoated 316 L disks. This was attributed to the formation of chromium oxide on coatings as Eq. (3), and then the anodic dissolution current decreased as indicated by the rise in the OCP [34]. When the carbon concentration gradually increased from 15.4 at.% to 75.0 at.%, the corresponding chromium concentration declined from 64.2 at.% (CrCN1) to 9.5 at.% (CrCN3). As a result, less chromium oxides could form on the CrCN coatings to hinder the penetration of electrolyte, which was proved by the values of $R_{po}$ (pore resistance) in Table 6. Thus, the OCPs of CrCN coatings declined as carbon concentration increased.

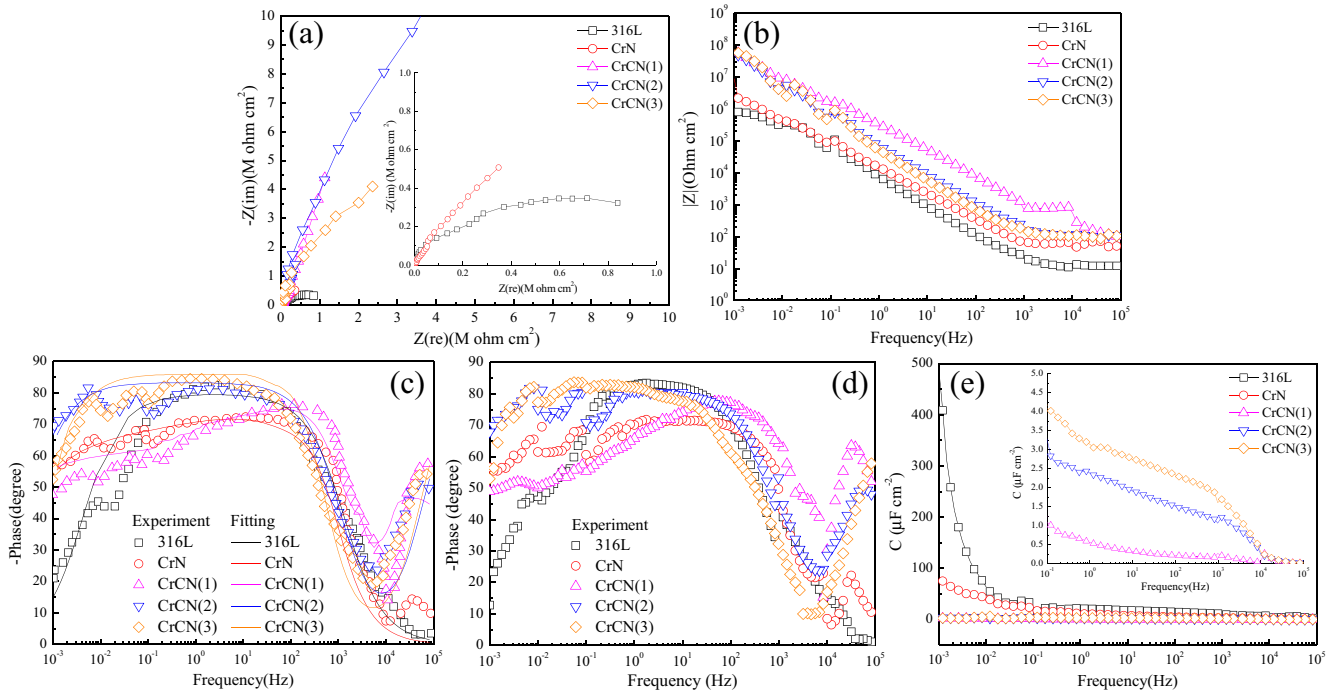


**Fig. 5.** (a) Nyquist plots, (b, c) Bode plots. (d) repetition and (e) interfacial capacitances as a function of frequency of the coated and uncoated 316 L disks.

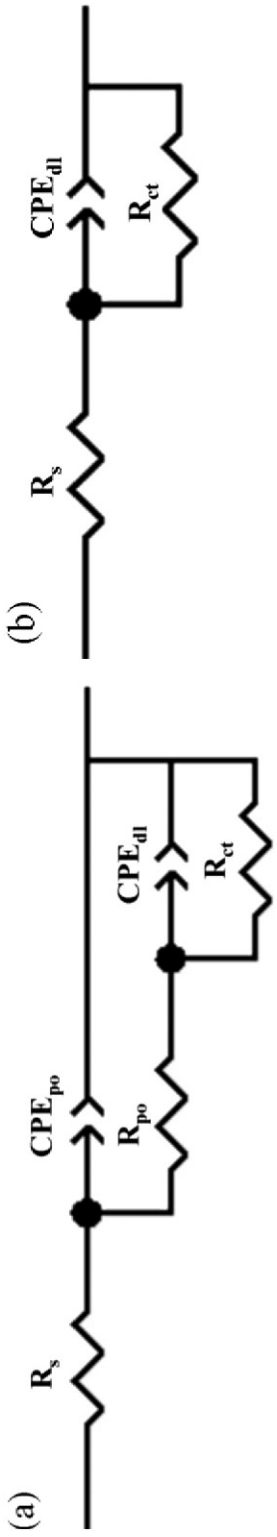


**Fig. 6.** Equivalent circuits for (a) the coated 316 L disk and (b) the uncoated 316 L disk.

### 3.3. Influence of carbon concentration on the EIS of CrCN coatings

The Nyquist plots of all specimens are illustrated in Fig. 5a, which presented similarly incomplete capacitive reactance arcs. As seen the inset in Fig. 5a, it is conspicuous that the uncoated 316 L disk exhibited the smallest capacitive reactance arc followed by CrN-coated 316 L disk. As the carbon concentrations were 15.4 at.% and 52.6 at.%, the diameters of capacitive reactance arcs for CrCN(1) and CrCN(2) coatings became large and seemed to be identical. But an obviously smaller diameter of capacitive reactance arc for the CrCN(3) coating was observed when the carbon concentration rose to 75.0 at.%. On the other hand, as seen in Fig. 5b, the uncoated 316 L disk displayed the lowest modulus of impedance (|Z|), while the CrN-coated 316 L disk in corresponding Bode plot showed a little higher |Z|. Although it was hard to distinguish the order of |Z| among CrCN coatings during low frequency region, the larger capacitive reactance arcs in Fig. 5a and the higher |Z| in Fig. 5b demonstrated that CrCN coatings could provide enhancing barrier effects as compared with uncoated and CrN-coated 316 L disks in SBF.

As seen in Fig. 5c, the experimental and fitting spectra were illustrated simultaneously, and the repetition of Bode plot in Fig. 5d was of little difference. Thus, the Bode plot in Fig. 5c would be described here. When CrN coating was deposited on 316 L disk, the phase between $10^{-1}$–$10^{2}$ Hz declined by about 10° as compared with that of uncoated 316 L, but the phase between $10^{-3}$–$10^{-1}$ Hz rose by a maximum of 35°. When the carbon content was 15.4 at.% in the CrCN coatings, there was a novel phase increment between $10^{1}$–$10^{3}$ Hz accompanying with slight phase drop between $10^{-3}$–$10^{1}$ Hz. Subsequently, when carbon concentration increased to 52.6 at.% and 75.0 at.%, the phases of CrCN(2) and CrCN(3) coatings between $10^{2}$–$10^{3}$ Hz went down even below that of uncoated 316 L, but the phases between $10^{-3}$–$10^{2}$ Hz became much higher. Generally, the enhancement of phase between $10^{-3}$–$10^{-1}$ Hz implied that the CrCN coatings were prone to performing as capacitances to prevent electrolyte from attacking over more broad frequency range. Fig. 5e shows the dependence of interfacial capacitance (C) as a function of frequency for all samples in SBF. It is obvious that the interfacial capacitance of CrCN coatings was proportional to carbon concentration. Especially, the lowest interfacial capacitance of CrCN(1) coating implied the lowest potential difference, which made the transports of point defects within passive layers harder and slower as compared with the rest of the samples [35].

By combining Bode plots with chi-square values ($\chi^2$) from ZsimpWin software testings [36,37], a frequently equivalent circuit with two time constants in Fig. 6a was introduced to depict the electrochemical processes of CrCN-coated 316 L disks [38]. On the contrary, an equivalent circuit with only one time constant in Fig. 6b was chosen to fit the electrochemical process of uncoated 316 L disk. In here, as a substitute of non-ideal capacitor, constant phase element (CPE) was used to describe the deviation from actual capacitive behavior [39]. Its impedance is expressed as:

$$Z_Q = 1/[Y_o(j\omega)^n] \quad (4)$$

where $Y_o$ is the capacitance (Fs $n^{-1}$ $m^{-2}$), ω is the angular frequency (rd/s), and n is the CPE power that represents the degree of deviation from a pure capacitor. For $n = 1$, Q is an ideal capacitor, while for $n < 1$, Q is non-ideal. In the equivalent circuit (EC), $R_s$, $R_{po}$ and $R_{ct}$ stood for electrolyte resistance, coating pore resistance and charge transfer resistance, respectively. Meanwhile, the corresponding coating capacitance and double-layer capacitance were symbolized as $CPE_{po}$ and $CPE_{dl}$.

After EIS data were fitted with ZsimpWin software, the respective values of each component are listed in Table 6. The unusual $R_s$ of 316 L disks coated with CrN and CrCN(2) coatings was ascribed to systemic error at high frequency while the rest of the $R_s$ varied in the range of 3–11 Ω cm$^2$ [40]. Although the CrN-coated 316 L disk showed lower electrical resistivity and looser topography than 316 L disk, the formation of chromium oxide during electrochemical process triggered the highest $R_{po}$ ($1.85 \times 10^2$ Ω cm$^2$) which directly contributed to corresponding higher $R_{ct}$. Subsequently, owing to the formation of a-$CN_x$ with N–C bonds alone at 15.4 at.% carbon incorporation and dense morphology with higher electrical resistivity, the 316 L disk coated with CrCN(1) coating exhibited higher $R_{ct}$ ($5.33 \times 10^7$ Ω cm$^2$) than CrN coated sample. However, for CrCN(2) and CrCN(3) coatings, the higher carbon concentration beyond 52.6 at.% made a-$CN_x$ component consist of N–C and N═C bonds simultaneously. Since the stability of N═C bonds was relatively weaker than that of N–C bonds, i.e., the π bond in N═C could be broken easily [41]. Thus, during corrosion process, the CrCN(2) and CrCN(3) coatings with N═C bonds would be inclined to be degraded more easily, so the samples coated with CrCN(2) and CrCN(3) exhibited lower $R_{ct}$ ($3.35 \times 10^7$ Ω cm$^2$ and $8.06 \times 10^6$ Ω cm$^2$).

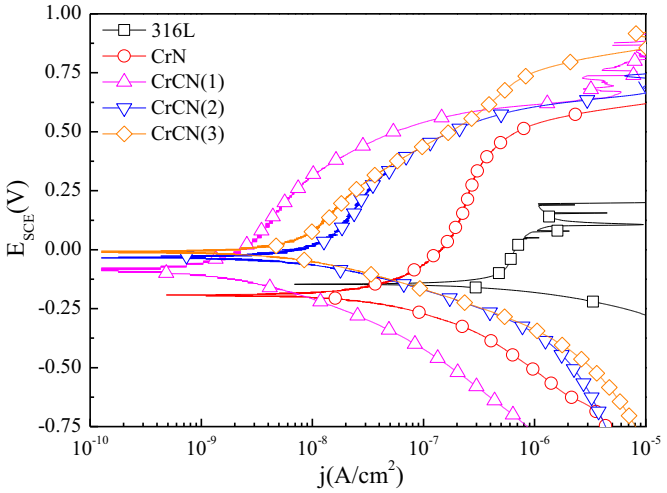


**Fig. 7.** Polarization curves of the coated and uncoated 316 L disks.

### 3.4. Evolution of potentiodynamic polarization

As seen in Fig. 7, the order of anode polarization current density was arranged as: 316 L > CrN > CrCN(2) > CrCN(3) > CrCN(1), which manifested favorable electrochemical properties of CrN and CrCN coatings. According to Tafel plot extrapolation, the $E_{corr}$, $j_{corr}$, $\beta_a$ and $\beta_c$ were obtained as well as $R_p$ by Eq. (2), and these values are listed in Table 7. It is clear that the 316 L disks coated with CrN or CrCN coatings displayed lower corrosion current densities (1.79–35.2 nA cm$^{-2}$) than those (773 nA cm$^{-2}$) of uncoated 316 L disk by one or two orders of magnitude. This implied that the corrosion rate of CrN or CrCN coatings was lower than that of 316 L disk during polarization process. For the CrN-coated 316 L disk, the inhibition effect of chromium oxide contributed to the corresponding $R_p$ of 999.6 kΩ cm$^2$, while denser topography and higher electric resistivity made $R_p$ of CrCN(1) coating (15.4 at.% C) increase to 22782.6 kΩ cm$^2$. And then, the $R_p$ of CrCN(2) and CrCN(3) coatings decreased to 3999.4 and 5218.6 kΩ cm$^2$ respectively because of the formation of vulnerable N═C bonds, when the carbon

**Table 7**
Results of potentiodynamic polarization tests.

| Samples | E vs SCE (V) | $j_{corr}$ (nA cm$^{-2}$) | $\beta_a$ (V) | $\beta_c$ (V) | $R_p$ (kΩ cm$^2$) |
|---|---|---|---|---|---|
| 316 L | −0.145 | 773 | 0.908 | 0.108 | 54.2 |
| CrN | −0.197 | 35.2 | 0.228 | 0.143 | 999.6 |
| CrCN(1) | −0.088 | 1.79 | 0.286 | 0.132 | 22782.6 |
| CrCN(2) | −0.037 | 9.06 | 0.310 | 0.119 | 3999.4 |
| CrCN(3) | −0.009 | 7.38 | 0.317 | 0.120 | 5218.6 |

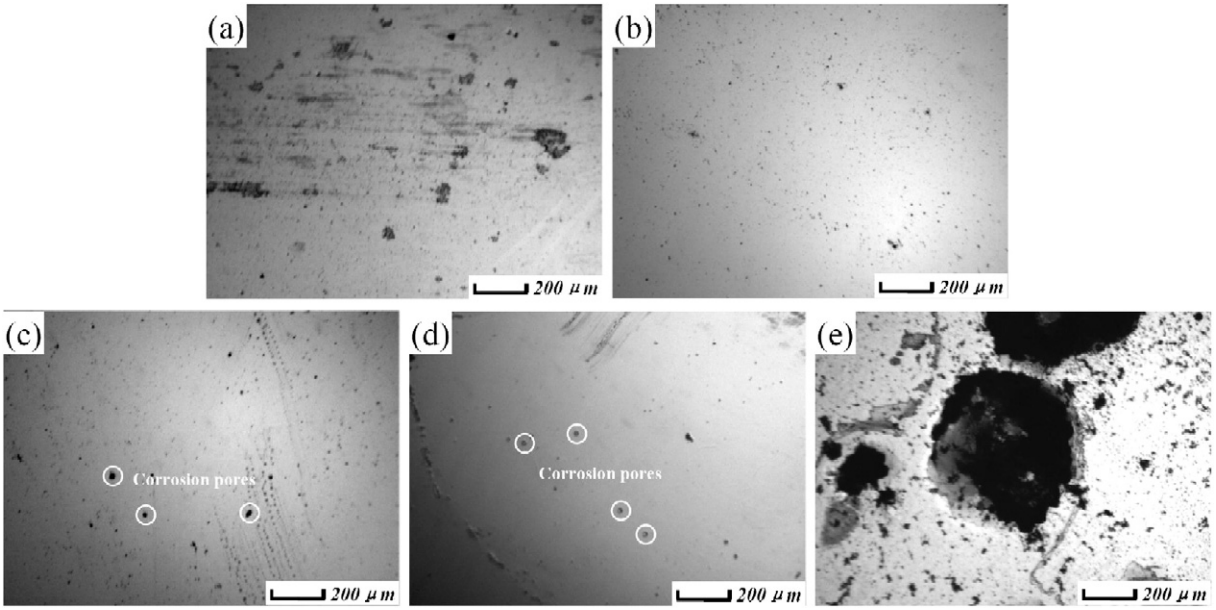


**Fig. 8.** Optical images of (a) CrN, (b) CrCN(1), (c) CrCN(2), (d) CrCN(3) and (e) 316 L after polarization tests.

concentration increased to 52.6 at.% and 75.0 at.%. However, all $R_p$ of CrN or CrCN coated 316 L disks were higher than that (54.2 kΩ $cm^2$) of uncoated 316 L disk.

The corresponding surface conditions after polarization test are shown in Fig. 8. It is obvious that the uncoated 316 L confronted serious etching with big corrosion pores left (Fig. 8e) due to poor inhibition. On the contrary, all coated samples remained integrity on account of superior electrochemical properties. Among them, the corrosion extent of CrN coated sample was severer than the rest accompanying with some corrosion area, while CrCN(1) coated sample exhibited best surface quality. Regarding CrCN(2) and CrCN(3) coated samples, some small corrosion pores presented on the surface after polarization test. Thus, taking the above results into account, all CrN or CrCN coated specimens exhibited better protection effect than those of uncoated 316 L which was consistent with EIS results. Especially, the CrCN(1) coating with N–C bonds alone was the best candidate to protect uncoated 316 L disk in this study.

## 4. Conclusion

The evolution of electrochemical properties of CrCN coatings as a function of carbon content in simulated body fluid (SBF) was evaluated, and the most favorable CrCN coating with 15.4 at.% carbon was able to enhance corrosion resistance of 316 L, which might prolong the longevity of femoral head prosthesis. The detailed conclusions are summarized as:

(1) The CrCN-coated 316 L disks displayed stronger protective abilities than the CrN-coated or uncoated 316 L disks, and were able to prolong service life of femoral head prosthesis to a certain extent.
(2) As the carbon concentration was 15.4 at.%, the CrCN(1)-coated 316 L disk possessed superior protective property in simulated body fluid owing to more a-$CN_x$ content with relatively stable N–C bond alone.
(3) As the carbon concentration increased to 52.6 at.% and 75.0 at.%, the protective effects of CrCN(2) and CrCN(3) coatings were gradually degraded owing to the formation of vulnerable N═C bond with easy breakage of π bond.

## Acknowledgment

This work was supported by National Natural Science Foundation of China (Grant No. 51375231), The Research Fund for the Doctoral Program of Higher Education (Grant No.20133218110030) and Priority Academic Program Development of Jiangsu Higher Education Institutions (PAPD). We would like to acknowledge them for their financial support.

## References

[1] D. Gopi, V.C.A. Prakash, L. Kavitha, Mater. Sci. Eng. C 29 (2009) 955–958.
[2] Y. Khelfaoui, M. Kerkar, A. Bali, F. Dalar, Surf. Coat. Technol. 200 (2006) 4523–4529.
[3] V. Singh, K. Marchev, C.V. Cooper, E.I. Meletis, Surf. Coat. Technol. 160 (2002) 249–258.
[4] J. Pellier, J. Geringer, B. Forest, Wear 271 (2011) 1563–1571.
[5] V. Muthukumaran, V. Selladurai, S. Nandhakumar, M. Senthilkumar, Mater. Des. 31 (2010) 2813–2817.
[6] F. Macionczyk, B. Gerold, R. Thull, Surf. Coat. Technol. 142–144 (2001) 1084–1087.
[7] D. Bociaga, K. Mitura, Diam. Relat. Mater. 17 (2008) 1410–1415.
[8] S. Carmignato, M. Spinelli, S. Affatato, E. Savio, Wear 270 (2011) 584–590.
[9] J. Geringer, W. Tatkiewicz, G. Rouchouse, Wear 271 (2011) 2793–2803.
[10] R. Crowninshield, A. Rosemberg, S. Sporer, Clin. Orthop. Relat. Res. 443 (2006) 266–272.
[11] P. Papakonstantinou, J.F. Zhao, P. Lemoine, E.T. McAdams, J.A. McLaughlin, Diam. Relat. Mater. 11 (2002) 1074–1080.
[12] R.C.C. Rangel, M.E.P. Souza, W.H. Schreiner, C.M.A. Freire, E.C. Rangel, N.C. Cruz, Surf. Coat. Technol. 204 (2010) 3022–3028.
[13] Q.Z. Wang, F. Zhou, Z.F. Zhou, C.D. Wang, W.J. Zhang, L.K.-Y. Li, S.-T. Lee, Electrochim. Acta 112 (2013) 603–611.
[14] R.A. Antunes, A.C.D. Rodas, N.B. Lima, O.Z. Higa, I. Costa, Surf. Coat. Technol. 205 (2010) 2074–2081.
[15] L.F. Senna, C.A. Achetea, T. Hirschb, F.L. Freire Jr., Surf. Coat. Technol. 94–95 (1997) 390–397.
[16] Q.Z. Wang, F. Zhou, Z.F. Zhou, L.K.-Y. Li, J.W. Yan, Surf. Coat. Technol. 253 (2014) 199–204.
[17] P.F. Hu, B.L. Jiang, Vacuum 85 (2011) 994–998.
[18] Q.Z. Wang, F. Zhou, X.D. Ding, Z.F. Zhou, C.D. Wang, W.J. Zhang, L.K.Y. Li, S.T. Lee, Appl. Surf. Sci. 268 (2013) 579–587.
[19] P.Y. Yi, L.F. Peng, T. Zhou, H. Wu, X.M. Lai, Int. J. Hydrog. Energy 38 (2013) 1535–1543.
[20] D.K. Merl, P. Panjan, M. Cekada, M. Macek, Electrochim. Acta 49 (2004) 1527–1533.
[21] S. Kaciulis, A. Mezzi, G. Montesperelli, F. Lamastra, M. Rapone, F. Casadei, T. Valente, G. Gusmano, Surf. Coat. Technol. 201 (2006) 313–319.
[22] C.Y. Chiang, Y. Shin, S. Ehrman, J. Electrochem. Soc. 159 (2012) B227–B231.
[23] P.J. Li, C. Ohtsuki, T. Kokubo, K. Nakanishi, N. Soga, J. Am. Ceram. Soc. 75 (1992) 2094–2097.
[24] B.A. Boukamp, J. Electrochem. Soc. 142 (1995) 1885–1894.

[25] C. Anandan, V.K. William Grips, V. Ezhil Selvi, K.S. Rajam, Surf. Coat. Technol. 201 (2007) 7873–7879.
[26] T. Polcar, L. Cvrček, P. Široký, R. Novák, Vacuum 80 (2005) 113–116.
[27] J.C. Walker, I.M. Ross, C. Reinhard, W.M. Rainforth, PEh. Hovsepian, Wear 267 (2009) 965–975.
[28] C. Barshilia Harish, K.S. Rajam, J. Mater. Res. 19 (2004) 3196–3205.
[29] F. Guinneton, O. Monnereau, L. Argeme, D. Stanoi, G. Socol, I.N. Mihailescu, T. Zhang, C. Grigorescu, H.J. Trodahl, L. Tortet, Appl. Surf. Sci. 247 (2005) 139–144.
[30] D. Stanoi, G. Socol, C. Grigorescu, F. Guinneton, O. Monnereauc, L. Tortetc, T. Zhangd, I.N. Mihailescu, Mater. Sci. Eng. B 118 (2005) 74–78.
[31] V. Ezirmik, E. Senel, K. Kazmanli, A. Erdemir, M. Urgen, Surf. Coat. Technol. 202 (2007) 866–870.
[32] H. Riascos, J. Neidhardt, G.Z. Radnóczi, J. Emmerlich, G. Zambrano, L. Hultman, P. Prieto, Thin Solid Films 497 (2006) 1–6.
[33] S. Kannan, A. Balamurugan, S. Rajeswari, Mater. Lett. 57 (2003) 2382–2389.
[34] N. Figueira, T.M. Silva, M.J. Carmezim, J.C.S. Fernandes, Electrochim. Acta 54 (2009) 921–926.
[35] L.L. Liu, J. Xu, P. Munroe, J.K. Xu, Z.H. Xie, Acta Biomater. 10 (2014) 1005–1013.
[36] J.H. Sui, W. Cai, Surf. Coat. Technol. 201 (2007) 6906–6909.
[37] R.Q. Hang, S.L. Ma, P.K. Chu, Diam. Relat. Mater. 19 (2010) 1230–1234.
[38] F. Mansfeld, J. Appl. Electrochem. 25 (1995) 187–202.
[39] C. Liu, Q. Bi, A. Leyland, A. Mattews, Corros. Sci. 45 (2003) 1243–1256.
[40] A. Zeng, E. Liu, S. Zhang, S.N. Tan, P. Hing, I.F. Annergren, J. Gao, Thin Solid Films 426 (2003) 258–264.
[41] J. Robertson, Mater. Sci. Eng. R 37 (2002) 129–281.